Available online at www.sciencedirect.com

ScienceDirect

journal homepage: http://www.elsevier.com/locate/acme

Original Research Article

Sequence of damage events occurring in the course of low energy impact

Piotr Czarnocki *, *Tomasz Zagrajek*

Institute of Aeronautics and Applied Mechanics, Warsaw University of Technology, Nowowiejska 24, 00 665 Warsaw, Poland

ARTICLE INFO

Article history:
Received 18 December 2015
Accepted 11 May 2016
Available online 14 July 2016

Keywords:
Impact
Laminates
Damage
Delamination
Simulation

ABSTRACT

Finite element simulation was carried out to better understand damage formation in CF/epoxy plate in the course of a low velocity 8J impact. The plate under investigation was of $[+30/-30]_s$ lay-up. To validate the numerical results a drop test was carried out with the help of a drop tower. The interlaminar damage extent was determined with the help of C-scan. Comparison between the numerical and experimental results showed a good quantitative agreement concerning contact force time history, however, the amount of dissipated energy determined based on the numerical simulation was lower than that from the experiment, consistently, the damage extent determined based on numerical simulation was smaller than that determined by C-scan. Nevertheless, characteristic points on the plot representing contact force time history could be related to the particular damage mechanism onsets and their actions.

1. Introduction

Often, service damage to composite airframes taking place during operation of an aircraft is caused by a low energy impact of a foreign object. Often, primary parts of composite airframes are of laminar structure, for which the interlaminar fracture resistance is the Achilles' heel since such impacts can easily produce delaminations accompanied by intralaminar fracture. The purpose of the presented work was to investigate the sequence of events taking place during such a damage formation to understand better its mechanism.

Some researchers claim that it is possible to take advantage of a quasi-static tests for analysing impact damage events and mechanisms of energy dissipatation assuming the same maximum values of contact force and impact energy [1–4], however, some other investigations indicate that the damage extent and damage modes present depend on impactor mass and impactor velocity even though impact energy is the same [5].

Because of the aforementioned ambiguous results the presented FE simulation of impact damage took into account dynamic effects.

The object of investigation was a laminate plate containing reinforcement layers oriented at ±30°. Such a reinforcement configuration can compromise on shear and normal strengths and stiffness offered by a structure with 0° and ±45° reinforcement orientation. The former can offer simplification of a manufacturing process due to a lower number of different reinforcement orientations and simpler placing process,

* *Corresponding author*. Tel.: +48 222345856.
E-mail address: pecz@meil.pw.edu.pl (P. Czarnocki).
http://dx.doi.org/10.1016/j.acme.2016.05.002

however, on the expense of mechanical properties. In general, the design of symmetric and balanced laminates is recommended to avoid shear-extensional and extensional-bending couplings which can produce undesirable deformations in the case of both the mechanical and thermal loadings. For this reason the structure under consideration was of $[+30/-30]_s$ layup. Recently, possibility of wide application of just bi-directional laminates has been investigated [6,7]. In fact, this investigation has been focused on thin ply laminates, nevertheless, bi-directional laminates made with plies of a conventional thickness can also be superior to those combining four reinforcement directions. Usually, a balanced, symmetric laminate used for airframes is at least of six layer layup $[0/+45/-45]_s$, that is, it consists of two more layers comparing to the $[+30/-30]_s$ one, therefore, the specific strength and stiffness of both the laminates are similar.

If a penetration is not present the damage caused by a low energy impact is basically confined to an interior of laminate and for this reason a direct monitoring and investigation of damage formation process is difficult. For this reason, to perform this task an advantage of numerical simulation was taken.

Impact modelling with the application of various methods has been presented in a large number of papers. Some early papers provided closed form formulas for the critical values of contact forces, P_c, [8,9] or energy needed for fibre fracture [10], or critical strain energy release values, G_c, corresponding to the onset of delamination. Some attempts were made to relate these force and energy values to the delamination area taking advantage of the Linear Fracture Mechanics [11]. Also, using analytical models the deflection time history and maximum impact force versus projectile velocity were determined for particular laminate structures [12]. Simple FE models did not consider neither damage initiation nor its evolution but they allowed for the determination of deflection versus time and contact force versus time relationships [13] and for the determination of stress distribution in a plate versus time [14]. More advanced FE models provided results on delamination extent assuming that it corresponded to the area over which certain failure criteria were met [15,16]. The aforementioned models did not account for neither damage evolution nor resulting aftereffects. To account for this the VCCT method was used and interlaminar fracture process was modelled to represent also the interfacial debonding [17,18]. However, there is some inconvenience inherently connected to this method consisting in the need for crack presence prior to the impact. Such difficulties were overcome by the use of damage mechanics (DM) for which this requirement did not have to be fulfilled. FE models taking advantage of DM can also provide for inter and intralaminar damage modes and such an approach seems to be, so far, most versatile one. To model the damage process one can use cohesive elements or contact elements with prescribed cohesive material properties [19] for which various traction-displacement relationships can be defined [20–24]. Discussion on the application of various traction-displacement relationships can be found in [25]. Very often due to its simplicity a bi-linear traction-displacement relationship, Fig. 1, is assumed for simulation of interfacial failure [26–28]. Use of cohesive elements or contact elements with prescribed cohesive material properties is not necessary to take advantage of DM [29]. An entire FE model can be composed of solid elements alone. In the case of solid elements, damage initiation and damage evolution modelling can be done in a similar way as in the case of interface elements [30–34]. For detection of damage initiation various damage criteria can be used [35–38]. Tsai-Wu [35], Hashin [36], Chang-Chang [37], Puck [38] criteria, are among most common. For damage evolution, various combinations of the Strain

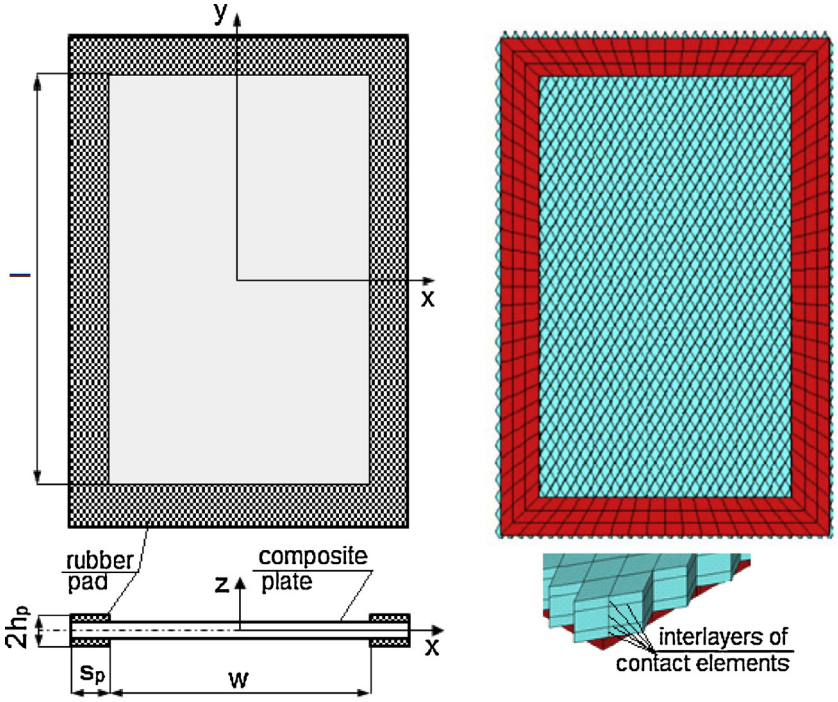

Fig. 1 – Modelled structure (a) and its FE representation (b).

Energy Release Rate values for fracture Mode I, II and III can serve this purpose [24]. Also, to model damage evolution the damage parameter values can be calculated with the help of chosen state variable e.g. equivalent stress using the modified Hashin criterion (LS-DYNA, Mat 162), [39]. Also, they can be defined in terms of strains [26,40].

In the presented study damage was modelled with the use of contact elements having prescribed cohesive zone material (CZM) properties. The study consisted of numerical and experimental parts.

2. Numerical studies

2.1. FE model

For numerical modelling of impact and damage evolution an implicit ANSYS FE code was used [41].

From the previous experimental work and inspections of the plates damaged by low energy impacts one concluded that two failure modes prevailed, namely delamination at interfaces of reinforcement layers differing by reinforcement orientation and intralaminar failure consisting in disbonding of matrix from fibres or/and in fracture of matrix between fibres.

To provide for such failure modes the developed FE model consisted of contact elements CONTA173 and Targe170 (according to ANSYS nomenclature) with prescribed CZM properties and solid rhombus brick elements SOLID185 (according to ANSYS nomenclature). The former were used to separate solid elements representing laminate from each other, i.e. to model delamination and intralaminar matrix failure. Choice of aforementioned geometry for brick elements allowed for overlapping the nodes of adjacent elements belonging to different sublaminates.

The main mechanism yielding energy dissipation is an interlaminar fracture which is triggered off by an intralaminar fracture modes such as matrix-fibre interface fracture or/and matrix fracture parallel to fibres. Fibre fracture is another intralaminar fracture processes. The reports available in the literature indicate that in the case of low energy impacts not causing laminate penetration fibre fracture is not extensive [42,43]. In addition, the amount of energy dissipated due to this process is not high because of carbon fibre fragility. It has not been reported, either, that fibre fracture itself can significantly initiate aforementioned damage processes. Therefore, the developed FE model did not account for fibre damage.

To facilitate experimental verification of the numerical results with the help of standard drop test [ASTM D7136/D7136M-07] the FE model geometry was chosen accordingly.

The assumed CZM material properties and material properties for solids are given in Table 1.

The modelled impacted rectangular 130 mm × 75 mm laminate plate was made from ETS/MTM46 carbon epoxy preimpregnates of $[+30/-30]_s$ layup. It resulted in a 4.2 mm thick laminate composed of three unidirectional sublaminates 1.05 mm, 2.1 mm and 1.05 mm thick. During the impact the plate was kept between two metal frames with rubber lining located along the edges of frames and separating the plate and metal frames from each other. The plate was subject to 8J impact exerted by the impactor ended with 12.5 mm diameter steel hemisphere and mass equal to 1.93 kg. It corresponded to the initial (contact) velocity equal to 2.88 m/s and to the drop high equal to 0.408 m.

2.1.1. Boundary conditions

The metal frames were not modelled. Instead, for the external surfaces of the rubber pads, i.e. for $z = \pm hp$ it was assumed that $uz = 0$, and the bounded contact was set at the rubber pad-composite interfaces. In addition, it was assumed that for $x = y = 0$ $ux = uy = 0$.

The FE mesh representing the plate and rubber pad is shown in Fig. 1.

2.2. Cohesive zone material behaviour in ANSYS

In the presented model the CZM behaviour was defined with the bi-linear traction-separation relationship sketched in Fig. 2. This relationship can be defined in several ways e.g. with the maximum stresses σ_{max}, t_{max} and corresponding gaps at completion of debonding separation δ_n^c, δ_t^c, respectively or alternatively with the maximum stresses σ_{max}, t_{max} and corresponding critical strain energy release rates G_{Ic} and G_{IIc}, respectively. The latter option was used for the presented FE model, Table 1. For a single fracture mode, e.g. Mode I the debondig parameter, d_n, can be defined as follows:

$$d_n = \left(\frac{\Delta_n - 1}{\Delta_n}\right)\chi \tag{1}$$

Table 1 – Mechanical properties of materials.

CZM		HTS/MTM46 laminate		Steel	Rubber
G_{Ic} [N/m]	100	E_{11} [GPa]	120.80	210.00	0.05
G_{IIc} [N/m]	900	$E_{22} = E_{33}$ [GPa]	8.12		
G_{IIIc} [N/m]	900	$G_{12} = G_{13}$ [GPa]	3.29		
σ_{1max} [MPa]	24	G_{23} [GPa]	1.60		
t_{2max} [MPa]	100	$\nu_{12} = \nu_{13}$	0.28	0.3	0 .48
t_{3max} [MPa]	100	X_T [MPa]	2036.50		
		X_C [MPa]	1116.00		
		Y_T [MPa]	24.80		
		Y_C [MPa]	180.00		
		S [MPa]	188.00		
		Density [kg/m^3]		7800.00	1250

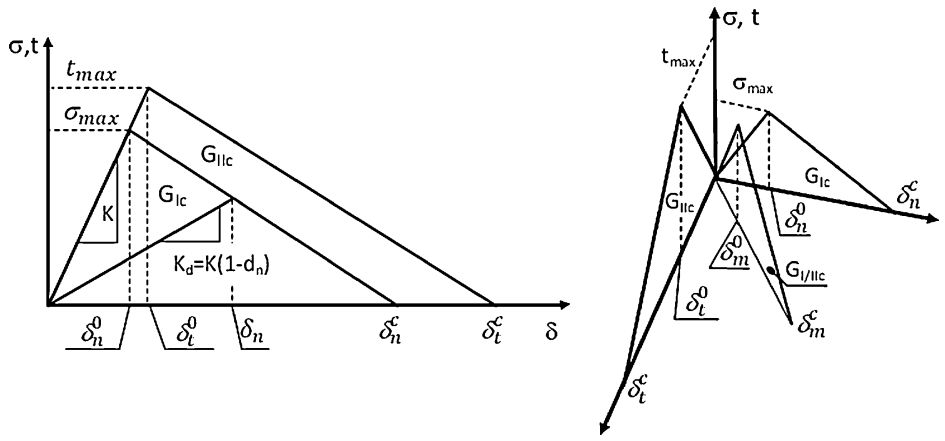

Fig. 2 – Parameters of cohesive zone material.

where: $\Delta_n = \frac{\delta_n}{\delta_n^0}$ and $\chi = \frac{\delta_n^c}{\delta_n^c - \delta_n^0}$

An additional condition on χ is put that

$$\chi = \frac{\delta_n^c}{\delta_n^c - \delta_n^o} = \frac{\delta_t^c}{\delta_t^c - \delta_t^o} \tag{2}$$

For any single fracture mode (e.g. Mode I) for traction range 0–σ_{max} deformation process is reversible. Irreversible damage process (softening) starts once a condition $\delta_n > \delta_{n0}$ is met. Damage evolution is defined by the damage parameter, d. It changes in a linear manner from 0 for $\delta_n = \delta_n^0$ and reaches 1 for $\delta_n = \delta_n^c$. In this range of displacement the stiffness K decreases according to (3):

$$K_d = K(1-d) \tag{3}$$

For Mixed-Mode I/II,by analogy, the debonding parameter, d_m, takes the form:

$$d_m = \left(\frac{\Delta_m - 1}{\Delta_m}\right)\chi \tag{4}$$

where: $\Delta_m = \delta_m / \delta_m^0$

It can be shown that

$$\delta_m^0 = \sqrt{(\delta_n^0)^2 (\delta_t^0)^2 \frac{1+\psi^2}{(\delta_t^o)^2 + \psi^2 (\delta_n^o)^2}} \tag{5}$$

where ψ is the mode mixity defined as follows: $\psi = \delta_t / \delta_n$.

Since for $\delta_m = \delta_m^f$ and $d_m = 1$, and bearing in mind condition (2) one can show that

$$\frac{\delta_n^o}{\delta_m^o} = \frac{\delta_n^f - \delta_n^o}{\delta_m^f - \delta_m^o} \tag{6}$$

Since G_c and σ_{max} are input data and δ_m^0 is given by (5) a gap opening, δ_m^f, at total decohesion can be calculated. It is assumed that the damage (or softening) starts if quadratic stress criterion

$$\left(\frac{\sigma}{\sigma_{max}}\right)^2 + \left(\frac{t}{t_{max}}\right)^2 \geq 1 \tag{7}$$

is met. Damage develops according to the Strain Energy Release Rate criterion and a total decohesion occurs if

$$\left(\frac{G_I}{G_{Ic}}\right)^2 + \left(\frac{G_{II}}{G_{IIc}}\right)^2 = 1 \tag{8}$$

3. Numerical results

Selected relevant results of the FE analysis are shown in Figs. 3 and 4 (with superimposed experimental result), in Figs. 5–7 (with superimposed experimental result), and 9.

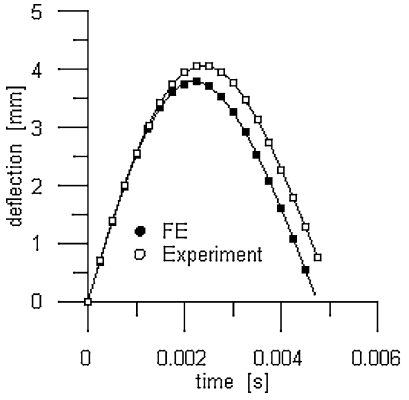

Fig. 3 – Maximum deflection of the plate at contact point vs. time.

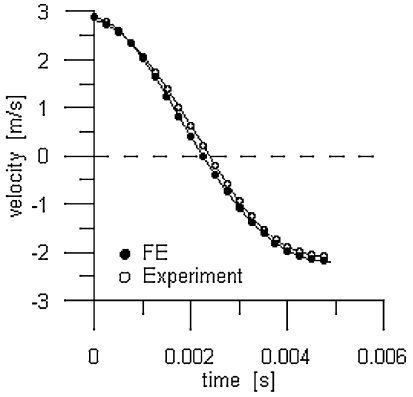

Fig. 4 – Impactor velocity vs. time.

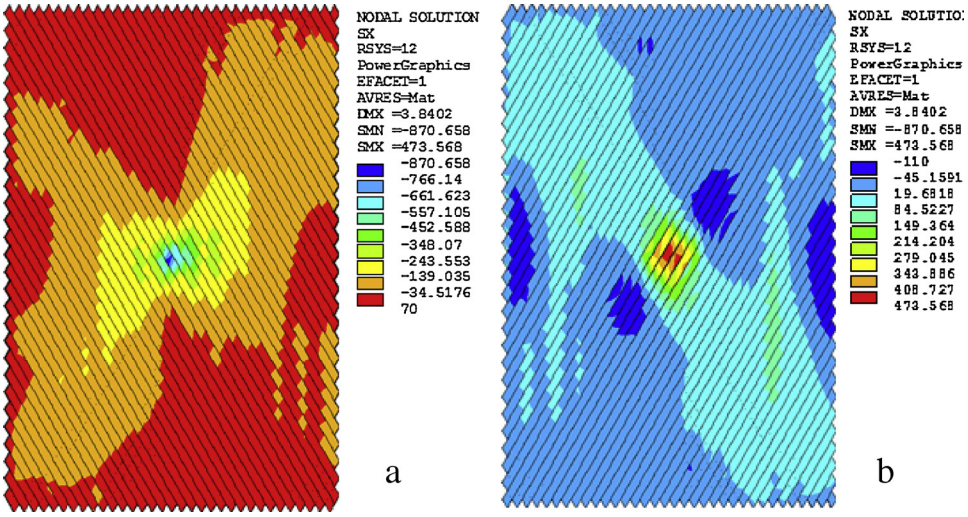

Fig. 5 – Stresses in the fibre directions in the most external layers (a) impacted layer, (b) bottom layer.

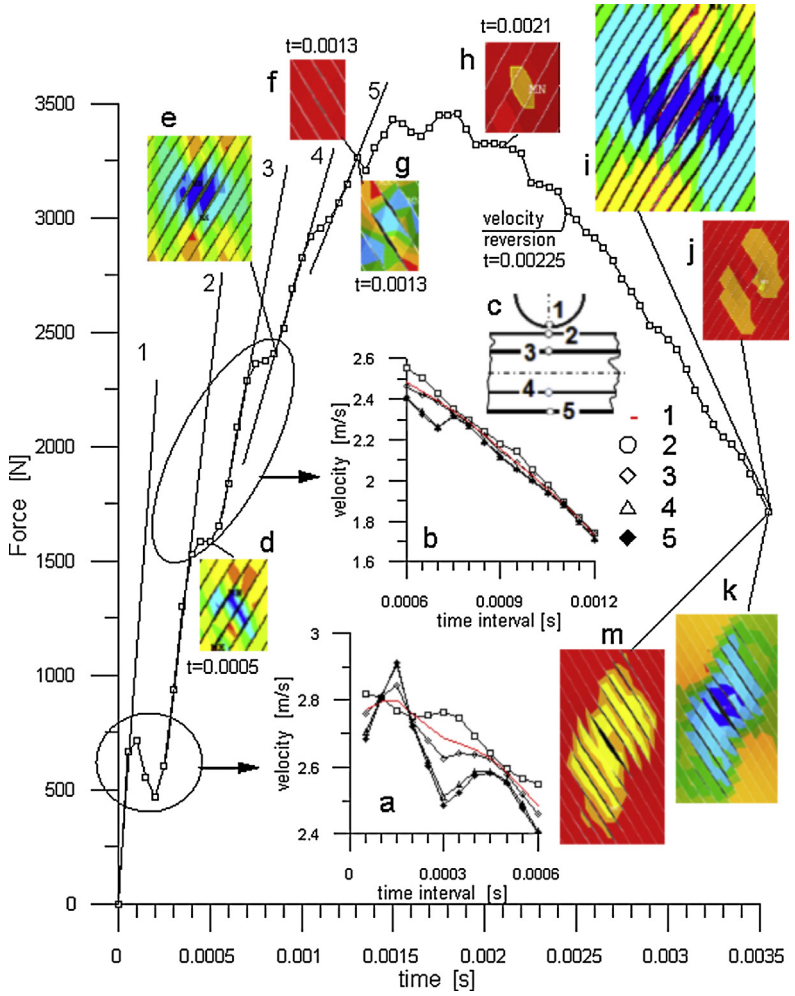

Fig. 6 – Force history; (a, b) diagrams showing nodal velocity divergence for nodes below the impactor; (c) node numbering; (d) first event of intralaminar failure in the bottom layer;(e) development of intralaminar damage in the bottom layer; (f–h) first event of delamination between the bottom and middle layers, intralaminar failure in the middle layer and delamination between the middle and top layers respectively; (i, k) overall extents of intralaminar damage in the bottom and middle layers, respectively; (j, m) overall delamination extents between the top-middle, and middle-bottom layers, respectively.

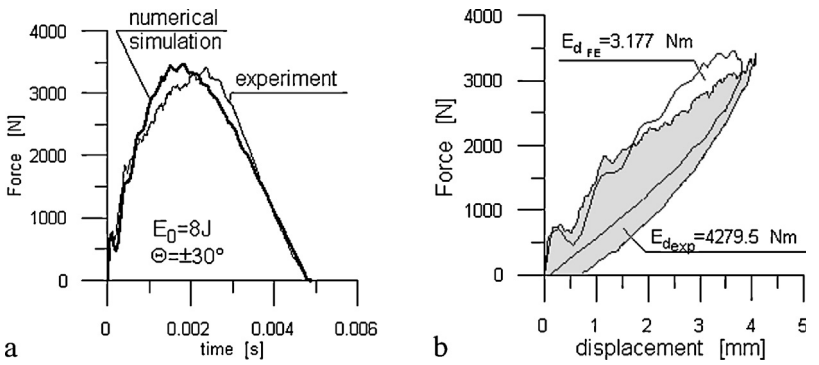

Fig. 7 – Superpostion of the experimental and FE simulation results; (a) force vs. time and (b) force vs. displacement plots (experimental results in grey).

Diagrams in Figs. 3 and 4 present the obtained deflection and velocity vs. time relationships. Contour plots in Fig. 5 present normal stresses in the fibre direction of the most external layers.

Essential outcome of the numerical simulation is the plot of contact force time history shown in Fig. 6. Inspecting the plot one could easily distinguish several almost straight line sections of varying slops denoted form 1 to 5. These sections were limited by the consecutive kinks occurring approximately for $t = 0.00015$ s, 0.00045 s, $t = 0.00075$ s, 0.00105 s, and 0.0013 s. The slopes of the sections decreased as force increased suggesting the occurrence of a successive reduction in the plate stiffness. It could possibly be attributed to the damage caused by the impactor or to the plate inertia, or to the both. To clarify this issue a velocity inspection of the impactor tip particles and plate particles located directly under the impactor tip was carried out for the time intervals corresponding to the kinks. For this purpose variation in velocity of the nodes located along z axis ($x = y = 0$), versus time was investigated. Respective plots have been superimposed on the main diagram. This inspection was supplemented with the inspection of plate integrity, i.e. checking whether any intra or interlaminar damage was present. For convenience, the time intervals of the first damage events, damage locations, and modes of damage have been shown on the same diagram. It was noticed that for $t = 0.00005$ s velocity of the plate nodes was lower than that of the impactor. For $t = 0.0001$ all the nodal velocities were approximately the same and for $t = 0.00015$ velocity of the plate nodes was higher than that of impactor tip. Such velocity variation corresponds to the first kink of force vs. time diagram i.e. for the first local drop of force that fall in 0.00015–0.0004 s time window. This force kinks separated first two diagram straight section of very similar slopes. However, one could notice that the first section was slightly steeper than the second one, in addition, lack of any damage evidence clearly suggested that the observed force variation with time was associated with the plate inertia. Initially, the impactor accelerated the resisting plate (initial force increase). This process was followed by a ''rebound'' and plate ''escape'' (force drop) and the consecutive impactor catching up with the plate (rise of force). After this series of events the plate was accelerated which was marked by an apparent drop of its stiffness. The second plot kink occurred in 0.00045–0.00055 s time window and the aforementioned pattern repeated. Divergence of nodes velocity decreased and then increased, i.e. velocity of the plate nodes was lower than that of impactor node. It was marked by an initial force plateau which was followed by a sharp increase in force gradient. Unlike for the previous kink the first damage event being intralaminar fracture of the bottom layer took place for $t = 0.0005$ s. Since that instant intralaminar damage of the bottom plate was continuously developing reaching its maximum extent for approximately $t = 0.0035$ s and remaining not changed till end of the impact simulation. Consequently, the onset of damage and damage development were marked by the decrease of slop of the straight line plot section falling in 0.0006–0.0007 s time window. Stage of intralaminar damage in the bottom plate for $t = 0.0013$ was shown next to the plot. It could be concluded that the stiffness drop that took place in 0.00045–0.0007 s time window could be attributed to both the inertia effect and initiation of intralaminar damage in the bottom layer. It could be noticed that with time the nodal velocities of the nodes under consideration equalized and the observed inertia effects were decreasing. Beyond $t = 0.0012$ s divergence of nodal velocities for nodes under consideration was negligible. Instead, the development of intralaminar damage in the bottom layer and emergence of new damage modes such as delamination between the bottom and middle layers and intralaminar failure in the middle layer were observed for $t = 0.0013$ s. The contact force reached its maximum for $t = 0.00185$ s. It was followed by an onset of delamination between the middle and top layers that occurred for $t = 0.0021$ s. The visible fluctuation of the contact force after extinction of the aforementioned inertia effect could be a resultant of damage development and free vibrations of already created plate fragments that interacted with each other coming in contact and losing it. Because the contact elements accounted for friction possible passing restoration of contact could affect the plate stiffness, however, such a phenomenon would be very difficult for tracking. The reversal of the impactor velocity occurred for $t = 0.00225$ s. Nevertheless, the impactor was still interacting with the plate exerting the decreasing contact force. The damage reached its maximum extent approximately for $t = 0.0035$ s and remained unchanged to the end of impact event.

4. Experimental work

4.1. *Experiments*

Experimental studies consisted of drop test and ultrasonic inspection of the resulting damage and determination of indentation profile in the plane parallel to fibres in the top layer. The drop test was carried out with the help of CAET 9050 Instron Drop Tower following the ASTM D7136/D7136M-07 standard recommendation. The ultrasonic inspection of post impact delamination geometry was investigated with C-scans taken with the help of a phased array ultrasonic technique. For this purpose the OmniScan SX flaw detector was used.

4.2. *Experimental results*

Experimental results concerning the drop test with superimposed corresponding numerical ones are shown in Figs. 3, 4 and 7. Fig. 8 presents indentation profile and Fig. 9c results of the ultrasonic inspection.

5. Discussion of results

Very good correlation between the experimental and numerical results was obtained for velocity time history, Fig. 4 and for the rising part of the deflection time history, Fig. 3 however, the remaining parts of diagrams slightly diverged.

In the case of contact force time history, Fig. 7, a good agreement between the maximum force values obtained from the FE simulation and drop test was reached. Also, a close resemblance of both the plots was clearly visible, especially for the initial time period up to the third plot kink. However, beyond the third plot kink some divergence between the experimental and numerical results was visible, i.e. general slope of the experimental contact force time history for the plot section limited by the third plot kink and maximum force value was lower than that of the corresponding section of the plot resulting from FE simulation. It indicated that the damage predicted by the FE simulation was underestimated. It was confirmed by the amounts of energy dissipated, Fig. 7b and C-scan shown in Fig. 9c. The amount of dissipated energy calculated from the test results was larger, (shown in grey in Fig. 7b) than that calculated based on FE simulation. The difference between the dissipated energy amounts determined from the experiment an from simulation seemed to be larger than the difference between the experimental and simulated contact force time histories. It could be justified by the fact that, in general, energy is a product of displacement and force. Changes of both the quantities with time differed, Figs. 3 and 7, concerning the experiment and numerical simulation and therefore their products differed to even the larger extent than did the contact force time histories alone. The results of ultrasonic inspection of delamination extents

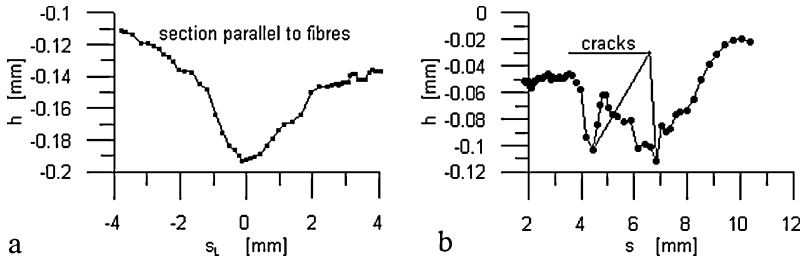

Fig. 8 – Profiles of permanent indentations, (a) parallel to fibres in section crossing the indentation centre, the smooth profile did not indicate fractured walls, (b) for comparison purpose: indentation with cracked walls – cracks indicated by the profile faults.

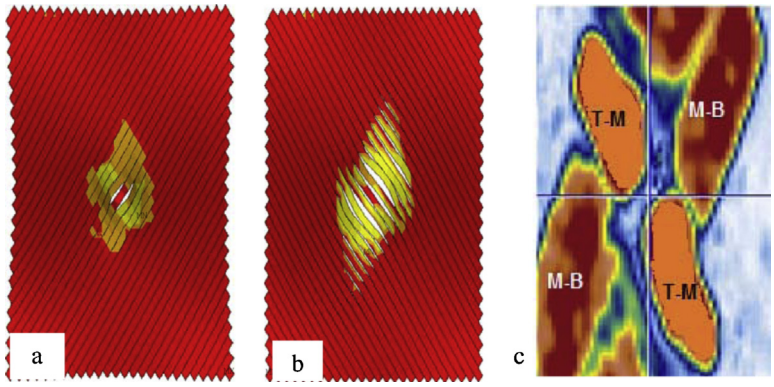

Fig. 9 – Final intra and interlaminar damages:(a) intralaminar damage in the top layer and delamination contour (in yellow) between top and middle layers; (b) intralaminar damage in the bottom layer and delamination contour (in yellow) between middle and bottom layers; (c) C-scan: delaminations between the top and middle layers (T–M), and between the middle and bottom layers(M–B).

between the top and middle layers (T–M) and middle and bottom layers (M–B) are shown in Fig. 9c and the corresponding results of FE analysis in Fig. 9a and b. The pictures were drawn to scale and reduce buy the same factor. Simple visual examination of the delamination areas determined numerically and experimentally allowed for conclusion that the results of numerical modelling yielded underestimation of the delamination extent which was in agreement with the results shown in Fig. 7b.

Not too many papers could be found on relating the contact force time history to particular damage events such as intra and interlaminar damages. The papers found presented results obtained for various boundary conditions which, in addition, were often not precisely reported. For this reason detailed comparison of the results reported in the literature to these presented in this paper was difficult. It could be stated that there was a general agreement that the first plot kink should not be associated with damage [33,44,45] and the next kink could be attributed to the delamination initiation [36] or matrix cracking [44]. In some cases the damage could be preluded by several oscillations followed by a sudden unstable delamination development [45].

Low energy impact damage consists of interlaminar fracture (delaminations) and intralaminar fracture. The latter can consist of fracture at matrix-fibre interface, fibre fracture and matrix, and permanent deformation. The main mechanism yielding energy dissipation is an interlaminar fracture triggered off by an intralaminar fracture modes such as matrix-fibre interface fracture or/and matrix fracture parallel to fibres. Fibre fracture is another intralaminar fracture processes. The reports available in the literature indicate that in the case of low energy impacts not causing laminate penetration fibre fracture is not extensive [42,43,24]. In addition, the amount of energy dissipated due to this process would not be high because of carbon fibre fragility. It has not been reported, either, that fibre fracture itself can significantly initiate aforementioned damage processes. In the case of the presented research, the performed stress analysis indicated that the highest normal stresses in the fibre direction in the most external layers, Fig. 5, were relatively low and did not exceed their ultimate values.

For the comparison purpose, the plots in Fig. 8 show slops of indentation profiles characteristic for indentations with intact, Fig. 8a, and fractured, Fig. 8b, walls. The indentation slopes shown in Fig. 8a are these of the indentation of the interest. They were smooth and did not provided evidence for noticeable fibre fracture. For the above-mentioned reasons the neglect of fibre fracture could be justified.

The results were obtained with the help of a relatively coarse FE mesh and should be treated with caution in quantitative terms, nevertheless, in qualitative terms they were self-consistent and were consistent with the experimentally determined contact force time history. Relatively large difference between the damage extent obtained based on FE simulation and the one from experiment could be attributed again to too coarse mesh of the FE model. Also, too coarse FE mesh is the most probably cause for the underestimation of dissipated energy amount. Unfortunately, the computing power available did not allowed for carrying out a simulation with the help of a finer mesh model.

6. Conclusions

Numerical simulation of impact damage evolution in a CF-epoxy laminate plate of $[+30/-30]_s$ lay-up was carried out with the help of FEM. The contact force, displacement and velocity time histories were of interest as well as the sequence and interaction of damage modes, and the damage extent. The numerical results were compared to the experimental ones.

For the velocity time history and the rising part of the deflection time history diagrams very good correlation between the experimental and numerical results was obtained, however, for the latter the remaining diagram parts slightly diverged.

For the contact force time histories a close resemblance of both the plots i.e. based on experiment and numerical simulation was clearly visible for the initial time period up to approximately 0.0011 s. The most pronounced divergence occurred for 0.011–0.0035 s time window, however a close agreement between the maximum values of the forces was obtain, nevertheless the pick force values were shifted by 0.0003 s, approximately. Good agreement between the experimental and numerical results was regained for the remaining time of the event.

The results of numerical simulation allowed for identification of the onsets of essential fracture events contributing to the laminate damage and for assigning them to the particular sections of the contact time history diagram. It was concluded that the first kink was due to the plate inertia and did not reflect any damage while the consecutive ones reflected onsets of the intralaminarr failure of bottom layer, delamination between the bottom and middle layers, intralaminar failure of the middle layer and delamination between the middle and top layer.

The computed maximum compressive and tensile stresses in the fibre direction never exceeded their ultimate values. This evidence for lack of fibre failure was supported by the appearance of the permanent indentation profile slops which were smooth and did not bear marks of fibre fracture, either. Nevertheless, an ultimate validation of an absence of meaningful fibre damage could be obtained by fractogrphic inspection.

In qualitative terms, the results of numerical simulation and experimental ones were consistent for entire force history, however, in quantitative terms they differed especially for the damage extent and amount of dissipated energy. These discrepancies could be attributed to too coarse FE mash. Unfortunately, the computing power available did not allowed for carrying out a simulation with the help of a finer mesh model.

Acknowledgement

The authors would like to thank Mrs. Dźwiarek for the proof reading of paper.

Funding: This study was supported by the grant no. N N504 4472 33.

REFERENCES

[1] E. Abisset, F. Daghia, X.C. Sun, M.R. Wisnom, S.R. Hallett, Interaction of inter- and intralaminar damage in scaled quasi-static indentation tests: part 1 – experiments, Composite Structures 136 (2016) 712–726.

[2] A. Wagih, P. Maimí, N. Blanco, J. Costa, A quasi-static indentation test to elucidate the sequence of damage events in low velocity impacts on composite laminates, Composites A 82 (2016) 180–189.

[3] A.T. Nettles, M.J. Douglas, in: A.T. Nettles, A. Zureick (Eds.), A Comparison of Quasi-Static Indentation Testing to Low Velocity Impact Testing, Composite Materials: Testing, Design, and Acceptance Criteria, ASTM STP 1416, American Society for Testing and Materials, West Conshohocken, PA, 2002.

[4] J.A. Artero-Guerrero, J. Pernas-Sánchez, J. López-Puente, D. Varas, Experimental study of the impactor mass effect on the low velocity impact of carbon/epoxy woven laminates, Composite Structures 133 (2015) 774–781.

[5] H. Zabala, L. Aretxabaleta, G. Castillo, J. Urien, J. Aurrekoetxea, Impact velocity effect on the delamination of woven carbon–epoxy plates subjected to low-velocity equienergetic impact loads, Composites Science and Technology 94 (2014) 48–53.

[6] S.W. Tsai, Weight and cost reduction by using unbalanced and unsymmetric laminates, in: 18th International Conference on Composite Materials, 21 August 2011–26 August, Jeju International Convention Center, Jeju Island, South Korea, 2011.

[7] P. Sanial, How C – Ply™ can change the way we design and manufacture, in: JEC Composites Innovative Composite Summit, Singapore, June, 2013.

[8] W. Cantwell, Geometrical effects in the low velocity impact response of GFRP, Composites Science and Technology 67 (9) (2007) 1900–1908.

[9] D.A.O. Davies, P. Robinson, Predicting failure by debonding/delamination, in: AGARD 74th Structures and Materials Meeting, 1992.

[10] G. Dorey, Impact damage in composites-development, consequences, and prevention, in: Proc of 6th Int. Conference on Composite Materials and 2nd European Conference on Composite Materials, vol. 3, Imperial College London, London, (1987) 3.1–3.26.

[11] G. Davies, X. Zhang, Impact damage prediction in carbon composite structures, International Journal of Impact Engineering 16 (1) (1995) 149–170.

[12] F. Mili, B. Necib, Impact behavior of cross-ply laminated composite plates under low velocities, Composite Structures 51 (3) (2001) 237–244.

[13] S. Khalili, M. Soroush, A. Davar, O. Rahmani, Finite element modeling of low-velocity impact on laminated composite plates and cylindrical shells, Composite Structures 93 (5) (2011) 1363–1375.

[14] C.N. Oguibe, D.C. Webb, Finite-element modelling of the impact response of a laminated composite plate, Composites Science and Technology 59 (12) (1999) 1913–1922.

[15] I. Choi, Low-velocity impact analysis of composite laminates under initial in-plane load, Composite Structures 86 (1–3) (2008) 251–257.

[16] Z. Aslan, R. Karakuzu, B. Okutan, The response of laminated composite plates under low-velocity impact loading, Composite Structures 59 (1) (2003) 119–127.

[17] R. Krueger, The virtual crack closure technique: history, approach and applications, in: NASA/CR-2002-211628 ICASE Report No. 2002-10, 2002, 1–59.

[18] S.J. Lord, M.F. Ngah, On the modelling of impact damage growth in composite structures, in: European Conference for Aerospace Science, 2005.

[19] S. Long, X. Yao, X. Zhang, Delamination prediction in composite laminates under low-velocity impact, Composite Structures 132 (2015) 290–298.

[20] A. Needleman, A continoum model for void nucleation by inclusion debonding, Journal of Applied Mechanics 54 (1987) 525–531.

[21] V. Tvergaard, J.W. Hutchinson, The influence of plasticity on mixed mode interface toughness, Journal of Mechanics and Physics of Solids 41 (1993) 1119–1135.

[22] W. Cui, M.R.A. Wisnom, A combined stress-based and fracture mechanics-based model for predicting delamination in composites, Composites 24 (1993) 467–474.

[23] Y. Mi, M.A. Crisfield, G.A.O. Davis, Progressive delamination using interface elements, Journal of Composite Materials 32 (1998) 1246–1272.

[24] N. Hongkarnjanakul, C. Bouvet, S. Rivallant, Validation of low velocity impact modelling on different stacking sequences of CFRP laminates and influence of fibre failure, Composite Structures 106 (2013) 549–559.

[25] H.D. Espinosa, S. Dwivedi, H. Lu, Modeling impact induced delamination of woven fiber reinforced composites with contact/cohesive laws, Computer Methods in Applied Mechanics and Engineering 183 (3–4) (2000) 259–290.

[26] D.J. Elder, R.S. Thomson, M.Q. Nguyen, M.L. Scott, Review of delamination predictive methods for low speed impact of composite laminates, Composite Structures 66 (1–4) (2004) 677–683.

[27] Y. Zhang, P. Zhu, X. Lai, Finite element analysis of low-velocity impact damage in composite laminated plates, Materials & Design 27 (6) (2006) 513–519.

[28] F. Aymerich, F. Dore, P. Priolo, Prediction of impact-induced delamination in cross-ply composite laminates using cohesive interface elements, Composites Science and Technology 68 (12) (2008) 2383–2390.

[29] C. Bouvet, S. Rivallant, J.J. Barrau, Low velocity impact modeling in composite laminates capturing permanent indentation, Composites Science and Technology 72 (2012) 1977–1988.

[30] L. Iannucci, Progressive failure modelling of woven carbon composite under impact, International Journal of Impact Engineering 32 (6) (2006) 1013–1043.

[31] P. Maimí, P.P. Camanho, J.A. Mayugo, C.G. Dávila, A continuum damage model for composite laminates: part I – constitutive model, Mechanics of Materials 39 (10) (2007) 897–908.

[32] M.V. Donadon, L. Iannucci, B.G. Falzon, J.M. Hodgkinson, S. de Almeida, A progressive failure model for composite laminates subjected to low velocity impact damage, Computers & Structures 86 (11–12) (2008) 1232–1252.

[33] C.S. Lopes, P.P. Camanho, Z. Gürdal, P. Maimí, E.V. González, Low-velocity impact damage on dispersed stacking sequence laminates. Part II: numerical simulations, Composites Science and Technology 69 (7–8) (2009) 937–947.

[34] S. Wang, L. Wu, L. Ma, Low-velocity impact and residual tensile strength analysis to carbon fiber composite laminates, Materials & Design 31 (1) (2010) 118–125.

[35] S.W. Tsai, E.M.G. Wu, A general theory of strength for anisotropic materials, Journal of Composite Materials 5 (1971) 58–80.

[36] Z. Hashin, Failure criteria for unidirectional fiber composites, Journal of Applied Mechanics 47 (1980) 329–334.

[37] F.K. Chang, K.Y. Chang, Post-failure analysis of bolted composite joints in tension or shear-out mode failure, Journal of Composite Materials 21 (1987) 809–833.

[38] A. Puck, H. Schurmann, Failure analysis of FRP laminates by means of physically based phenomenological models, Composites Science and Technology 62 (2002) 1633–1662.

[39] L. Maio, E. Monaco, F. Ricci, L. Lecce, Simulation of low velocity impact on composite laminates with progressive failure analysis, Composite Structures 103 (2013) 75–85.
[40] Y. Shi, T. Swait, C. Soutis, Modelling damage evolution in composite laminates subjected to low velocity impact, Composite Structures 94 (9) (2012) 2902–2913.
[41] Ansys, Release 14.5, Ansys, Inc., 2012, pp. 159–162.
[42] A. Ahmed, L. Wei, The low-velocity impact damage resistance of the composite structures – a review, Reviews on Advanced Materials Science 40 (2015) 127–145.
[43] M. Grasso, F. Penta, G.P. Pucillo, F. Ricci, V. Rosiello, Low velocity impact response of composite panels for aeronautical applications, in: Proceedings of the World Congress on Engineering, vol. II, London, UK, 2015.
[44] A. Riccio, A. de Luca, G. di Felice, F. Caputo, Modelling the simulation of impact induced damage onset and evolution in composites, Composites B 66 (2014) 340–347.
[45] G.A. Schoeppnera, S. Abrateb, Delamination threshold loads for low velocity impact on composite laminates, Composites A 31 (2000) 903–915.